IRIA

CENTRE
SOPHIA ANTIPOLIS

Institut National
de Recherche
en Informatique
et en Automatique

Domaine de Voluceau
Rocquencourt
BP 105
78153 Le Chesnay Cedex
France
Tel. (3) 954 90 20

Rapports de Recherche

N° 442

FINITE ELEMENT AND MULTIGRID SOLUTION OF THE TWO DIMENSIONAL EULER EQUATIONS ON A NON STRUCTURED MESH

Eric PEREZ

Septembre 1985

FINITE ELEMENT AND MULTIGRID SOLUTION OF THE TWO DIMENSIONAL EULER EQUATIONS ON A NON STRUCTURED MESH

E. PEREZ

Avions Marcel Dassault, Breguet Aviation,
DEA-DGT, 78 quai Carnot, 92214 St-Cloud, FRANCE.

SUMMARY

The two dimensional Euler equations are solved on non structured grids combining a Galerkin Finite Element approximation and a multigrid technique.

First a second order, centered, explicit scheme is derived from a Galerkine approach. The Multigrid implementation is then presented and some numerical results are discussed to validate the efficiency of the method.

RESUME

Les équations d'Euler bidimensionnelles sont résolues numériquement sur des maillages non structurés en combinant une approche Elément Finis de type Galerkine et une méthode multigrille. Un schéma explicite centré, précis au second ordre est d'abord déduit d'une formulation de type Galerkine.

L'algorithme multigrille et son implémentation sont ensuite présentés avec quelques résultats numériques pour démontrer ses performances.

FINITE ELEMENT AND MULTIGRID SOLUTION OF THE TWO DIMENSIONAL EULER EQUATIONS ON A NON STRUCTURED MESH

E. PEREZ

Avions Marcel Dassault, Breguet Aviation,
DEA-DGT, 78 quai Carnot, 92214 St-Cloud, FRANCE.

1. INTRODUCTION

Multigrid method for solution of the two dimensional Euler equations was shown to be highly sucessfull when coupled with finite volume approximations on structured quadrilateral or triangular grids [7], [9], [10].

The idea is to use corrections obtained on a coarse grid for the solution on a finer one. These corrections, derived from the problem equations, do not affect the accuracy of the fine grid solution but significantly increase the rate of convergence of the basic numerical scheme.

In the case of structured grids, computational coordinates which correspond to different grid lines can be defined . Therefore a coarser grid level is simply obtained by dropping every other grid line of a finer one. This allows uniform interpolation when transferring information from one grid to another. This

approach has to be modified to handle fully unstructured triangular meshes where the computational nodes are located by indirect adressing. This work is a first effort in this direction. In order to keep uniform interpolation between different grid levels, a multi-level-grid is generated by successive refinements, starting from a carefully chosen coarse grid. As a finite element method does not rely on the mesh structure, refinements can be global or local, leading to a global or local multi-level-grid. The multigrid algorithm treats these two cases the same way with no special treatment of the local mesh refinements. This seems promising for three dimensional computations for which the node number around complex geometries is critical.

2. NUMERICAL SCHEME

2.1 Euler Equations.

The two dimensional Euler equations are written in conservative form as :

$$(1) \quad \frac{\partial W}{\partial t} + \frac{\partial F}{\partial x} + \frac{\partial G}{\partial y} = 0$$

where

$$W = \begin{bmatrix} \rho \\ \rho u \\ \rho v \\ \rho E \end{bmatrix} \quad , \quad F = \begin{bmatrix} \rho u \\ \rho u^2 + p \\ \rho uv \\ \rho u(E + \frac{p}{\rho}) \end{bmatrix} \quad , \quad G = \begin{bmatrix} \rho v \\ \rho uv \\ \rho v^2 + p \\ \rho v(E + \frac{p}{\rho}) \end{bmatrix}.$$

The pressure p, the density ρ , the total energy E and the cartesian velocity components are assumed to satisfy the perfect gas state equation :

$$(2) \quad \rho E = \frac{p}{\gamma - 1} + \frac{1}{2}\left[u^2 + v^2\right]$$

where γ is the specific heat ratio.

2.2 Finite Element Approximation

In order to discretize the continuous problem, the flow region is imbedded in a large bounded polygonal domain Ω^h whose boundary are denoted by $\Gamma = \Gamma_b \cup \Gamma_\infty$. A triangulation T^h with characteristic mesh spacing h is introduced on Ω^h . The vertices of the triangles define a set of computational nodes, S^h , where the numerical solution of (1) is to be computed. For each node S_i , a piecewise linear basis function $N_i^h(x,y)$ of support Ω_i^h is introduced as shown on figure 1. It is a first degree polynomial on each element T_k of T^h which takes the value 0 for

all the nodes exept for S_i where $N_i^h(x_i,y_i) = 1$.

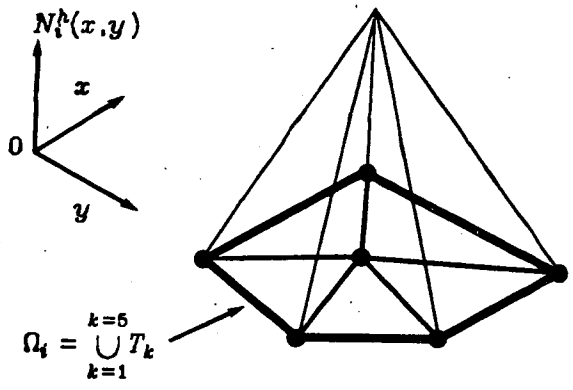

Figure 1 : Basis Function N_i^h

Any scalar function $\Phi(x,y)$ on Ω can be approximated as :

$$(3) \quad \Phi(x,y) = \sum_i N_i^h(x,y)\Phi(x_i,y_i)$$

where the sum is over all the nodes of S^h . In practice, the sum reduces to :

$$(4) \quad \Phi(x,y) = \sum_{i=1}^{i=3} N_i^h(x,y)\Phi(x_i,y_i)$$

where only the vertices of the element which contains point (x,y) are considered. In the remaining part, all the state variables will be represented by equation (4). Using the basis functions as weighting functions in the Galerkin approach, discrete equations are obtained by multiplication of equation (1) by $N_i^h(x,y)$ and integration by part.

$$(5) \quad \int\int_\Omega \left[\frac{W^{n+1}-W^n}{\Delta t}\right] N_i^h d\Omega = \int\int_\Omega \left\{F\frac{\partial N_i^h}{\partial x} + G\frac{\partial N_i^h}{\partial y}\right\} d\Omega - \int_\Gamma N_i^h \left[F\ n_x + G\ n_y\right] d\Gamma$$

where Δt is a time discretization step and $\vec{n}=(n_x,n_y)$ is the outward unit vector normal to Γ . Since the left hand side of equation (5) involves values of the state variables for all the nodes lying in Ω_i^h , the resulting system is of implicit nature. In order to allow explicit time integration of (5), a mass lumping operator L , is conveniently introduced so that the left hand side of (5) is replaced by :

$$(6)\quad \int\int_{\Omega} L\frac{W^{n+1}-W^{n}}{\Delta t}N_i^h d\Omega = \frac{area(\Omega_i^h)}{3}\left[\frac{W_i^{n+1}-W_i^{n}}{\Delta t}\right]$$

This approximation does not affect the steady state solution. The right hand side of equation (5) is discretized as follows :

$$(7)\quad \int\int_{\Omega}\left[F\frac{\partial N_i^h}{\partial x}+G\frac{\partial N_i^h}{\partial y}\right]d\Omega = \sum_{j.T_j\in\Omega_j} A_j\left[F_j\left[\frac{\partial N_i^h}{\partial x}\right]_j + G_j\left[\frac{\partial N_i^h}{\partial x}\right]_j\right]$$

where the sum is over all the elements connected to node i. The basis function derivatives are geometrical constants on each element and A_j is the area of element T_j . The mean fluxes F_j and G_j are computed by simple averaging of the nodes values as depicted on figure 2 :

$$F_j = F(\frac{1}{3}\sum_{i=1}^{i=3} W_i)\ ,\ G_j = G(\frac{1}{3}\sum_{i=1}^{i=3} W_i)$$

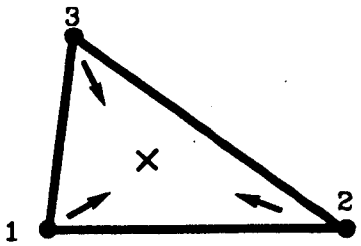

Figure 2 : Fluxes on element T_j

2.3 Boundary Conditions

The boundary conditions are taken into account by means of the boundary integral in equation (5) :

$$(8)\quad \int_{\Gamma} N_i^h\left[F\ n_x + G\ n_y\right]d\Gamma$$

On a solid body, the no-flux condition is specified and only the pressure term contributes to (8). Discretization is the following :

$$(9)\quad \int_\Gamma N_i^h \left[F\, n_x + G\, n_y \right] d\Gamma = \frac{1}{2} \sum_{j,\partial\Gamma_j \cap \Gamma_b \neq 0} \left[F_j N_x + G_j N_y \right]$$

where the sum is over elements which have an edge belonging to the solid boundary Γ_b . The contribution of such an element is given by :

$$(10)\quad F_j N_x + G_j N_x = \begin{bmatrix} 0 \\ p_j N_x \\ p_j N_y \\ 0 \end{bmatrix}$$

where p_j is the mean pressure on the boundary as depicted on figure 3 :

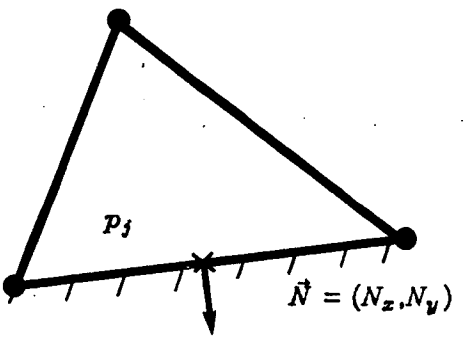

Figure 3 : Boundary Element

At infinity the boundary conditions are self imposed by an upwinding technique detailed in [2] which selects the right number of conditions depending on the local Mach number.

2.4 Pseudo-Time Integration

As described in the previous section, discretization of equation (5) leads to the following explicit scheme :

$$(11)\quad \frac{area\,(\Omega_i^h)}{3} \frac{W^{n+1} - W^n}{\Delta t} = Q^h(W^n)$$

where the spatial operator Q^h is a centered approximation of the right hand side of equation (5). In order to avoid spurious oscillations and overshoots in the vicinity of shocks or stagnation points in the numerical discrete solution, it is necessary to add an artificial viscosity term in the above scheme. A very simple Laplacian type model is considered by solving the following system via a variational formulation :

$$(12)\quad \begin{cases} \overline{W} = W + \varepsilon\left[\dfrac{\Delta x^2}{2}\dfrac{\partial^2 W}{\partial x^2} + \dfrac{\Delta y^2}{2}\dfrac{\partial^2 W}{\partial y^2}\right] \\ \overline{\overline{W}} = \overline{W} + \varepsilon\left[\dfrac{\Delta x^2}{2}\dfrac{\partial^2 \overline{W}}{\partial x^2} + \dfrac{\Delta y^2}{2}\dfrac{\partial^2 \overline{W}}{\partial y^2}\right] \end{cases}$$

which is equivalent to :

$$(13)\quad \overline{\overline{W}} - W = \varepsilon\left[\Delta x^2\frac{\partial^2 W}{\partial x^2} + \Delta y^2\frac{\partial^2 W}{\partial y^2}\right] + \frac{\varepsilon^2}{4}\left[\Delta x^4\frac{\partial^4 W}{\partial x^4} + \Delta y^4\frac{\partial^4 W}{\partial y^4}\right] + \varepsilon^2\frac{\Delta x^2\Delta y^2}{4}\frac{\partial^4 W}{\partial x^2\partial y^2}$$

where the smoothing parameter ε has to be tuned up with numerical experiment. Obviously such a model is not very sophisticated but preserves the accuracy of the scheme and introduces fourth order derivatives with little cost. Adaptation of ε with local gradients should be part of further developements. Discretization of (12) results in :

$$(14)\quad \overline{\overline{W}}^n - W^n = \Delta t\, D^h(W^n)$$

The solution is advanced in time using a Runge Kutta type multistage scheme as follows :

$$(15)\quad \begin{cases} W^0 = W^n \\ W^1 = W^0 - \alpha_1\,\Delta t\, R^h(W^0) \\ W^2 = W^0 - \alpha_2\,\Delta t\, R^h(W^1) \\ W^3 = W^0 - \alpha_3\,\Delta t\, R^h(W^2) \\ W^4 = W^0 - \alpha_4\,\Delta t\, R^h(W^3) \\ W^{n+1} = W^4 \end{cases}$$

where the residual $R^h(W)$ is defined by :

$$(16) \quad R^h(W^p) = Q^h(W^p) + D^h(W^0) \qquad p = 0,1,2,3$$

For economy, the smoothing operator is computed only once per multistage cycle. In addition, local time step is used to accelerate convergence to steady state. Current coefficients are chosen according to A. Jameson's stability analysis [8] :

$$(17) \quad \alpha_1 = .25 \quad \alpha_2 = .50 \quad \alpha_3 = .55 \quad \alpha_4 = 1.0$$

3. MULTIGRID SCHEME.

3.1 Algorithm

General equations of the multigrid theory can be found in many references and are not derived here. The guide line of this work is extensively detailed in reference [1].

From a triangulation T^H of Ω , a new finer triangulation T^h is obtained by subdividing some elements of T^H into two or four new elements. In the case of curved frontiers, nodes are replaced on the body as shown on figure 4. The choice of the elements to be subdivided is arbitrary and can depend on any imposed geometrical or physical criteria. If all the elements of T^H are subdivided (in four), the pair (T^H,T^h) is a global multi-level-grid. Otherwise the pair (T^H,T^h) is a local multi-level-grid. In this last case, some interface elements have to be divided into two new elements (see figure 4).

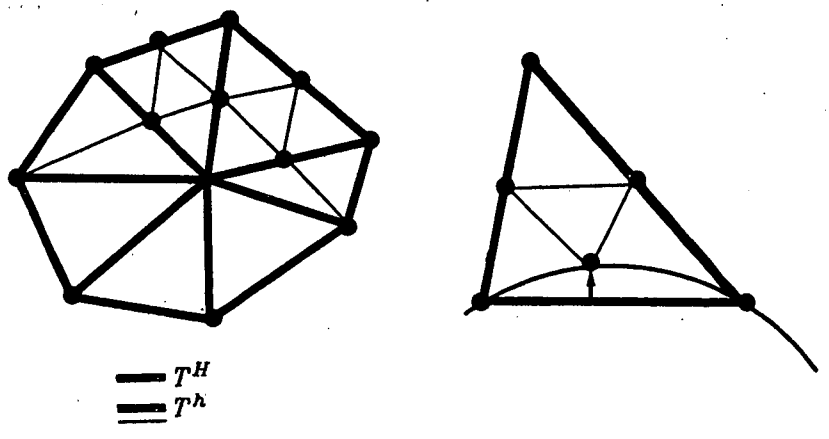

Figure 4 : subdivision

The system to be solved on T^h is written :

$$(18) \quad Q^h(W) = 0$$

Let us consider W^h an approximation of the solution of (18) obtained after some relaxation cycles as described in section 2.4. A new approximation of the solution can be obtained on T^H by solving :

$$(19) \quad Q^H(W^H) = \tau_h^H$$

where the source term τ_h^H is defined as :

$$(20) \quad \tau_h^H = \overline{I}_h^H R^h(W^h) - R^H(I_h^H W^h)$$

The operators $\overline{I}_h^H$ and I_h^H project quantities from grid T^h to grid T^H . Equation (19) is integrated with the scheme described in section 2.4 where the source term is easily included in the residual given in equation (16). The new approximation W^H obtained with (19) is projected back on T^h as follows :

$$(21) \quad W_{new}^h = W^h + I_H^h(W^H - I_h^H W^h)$$

The different projection operators constructed with the Finite Element interpolation spaces are described thereafter.

3.2 Solution Injection Operator I_h^H

Since each node of S^H belongs also to S^h , I_h^H is a straight injection which requires no operation.

3.3 Correction projection operator I_H^h

The natural choice is given by the basis functions as described in equations (3) and (4) :

$$(22)\quad \left[I_H^h W^H\right]_i = \sum_{j \in S^H} N_j^H(x_i, y_i) W_j^H$$

3.4 Residual Collection Operator $\overline{I}_h^H$

The difference between T^H and T^h does not only affect the mesh spacing size but also the corresponding sets of basis functions. In order to be consistent, $\overline{I}_h^H$ represents the residual computed on grid T^H with quantities obtained on grid T^h as mentioned in reference [6]. Therefore :

$$(23)\quad \left[\overline{I}_h^H R^h\right]_i = \int\int_\Omega I_h^H N_i^H \left[\frac{\partial F}{\partial x}(I_h^H W^h) + \frac{\partial G}{\partial y}(I_h^H W^h)\right] d\Omega$$

which reduces to :

$$(24)\quad \left[\overline{I}_h^H R^h\right]_i = \sum_{k \in \Omega_i^H} N_i^H(x_k, y_k) R_k^h$$

where the sum collects fine grid residual R_k^h for the nodes which lie in the support Ω_i^H of the basis function N_i^H.

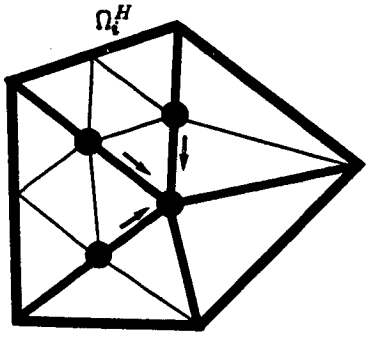

Figure 5 : Residual Collection

On figure 5 the sum is over nodes marked ● for which $N_i^H(x_k, y_k) = \frac{1}{2}$ and node S_i for which $N_i^H(x_i, y_i) = 1$.

3.5 Implementation.

The first step is to build a multi-level-grid. Typically, three grid levels are obtained by successive local or global refinements. The process described in part 3.1 is repeated on successively coarser grid levels. For each level, the solution of equation (19) is advanced in time with one multistage cycle followed by residual collection. The solution is injected on a coarser level and the process is repeated until the coarser grid is reached. At this point, corrections are interpolated back on successively finer levels using equation (21) until the finer grid is reached. This strategy is often refered to as the "saw tooth" technique.

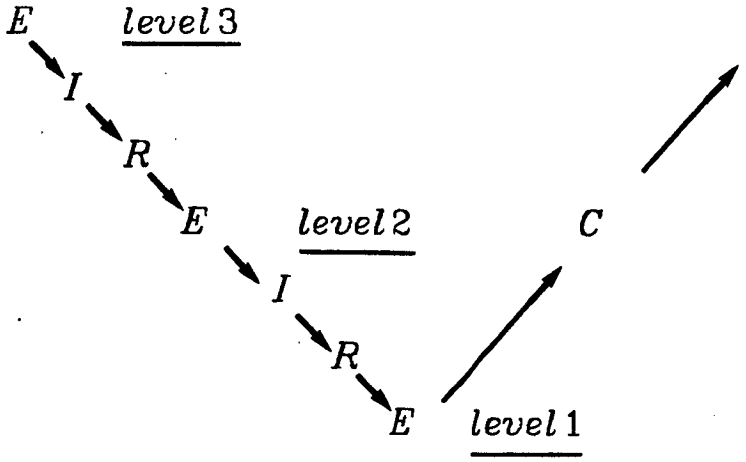

Figure 6 : Multigrid Cycle

4. RESULTS

4.1 Subsonic and Transonic flow in a bumped channel.

Figures 7 to 12 show results for the numerical simulation of flow in a channel with a circular bump at subsonic and transonic regimes. Successive grid levels are presented, starting with 161 nodes and 264 elements for the coarser one and ending with 2225 nodes and 4224 elements for the finer one. Convergence

histories are compared with the case where multigrid strategy is not used. The convergence rate is measured in terms of equivalent cycle which corresponds to the number of flux calculation required for one multistage cycle on the finer grid. In the current version of the code, one multigrid iteration was found to be theoretically equivalent to 1.66 multistage iteration. In terms of CPU time, one multigrid iteration represents approximately 2 multistage iteration. Grid handling is required only for corrections interpolation and represents only 1.8% of one multigrid iteration. Therefore the remaining time is consumed for fluxes and residual computation. Mach number on the lower wall is presented on figures 10 and 11 and entropy contours for the transonic case on figure 12. For the subsonic case, entropy production was found to be less than 0.08%.

4.2 Lifting Transonic Flow Around a NACA0012 Profile

Figures 13 to 18 show the results for the numerical simulation of a lifting transonic case around a NACA0012 profile. As for the previous case, the solution was obtained with a global multi-level-grid. Initial and final levels are presented and convergence history is compared with the case with no multigrid. Mach number and entropy contours show some preshock oscillations and entropy creation at the leading edge. This demonstrates the weakness of the artificial viscosity model but does not affect the conclusions about multigrid since the same solution is obtained without multigrid.

4.3 Transonic Case For Local Multigrid

Finally figures 19 to 21 demonstrate the ability of multigrid to include local adaptative mesh refinement. The first level is the same than for the previous case. The second level was obtained by refining only the elements in a fixed rectangle around the profile. The third level was obtained by refining only the elements on the profile and around the shock.

5. CONCLUSION

First numerical experiments have shown that multigrid method with Finite Elements can provide efficient solutions of the Euler equations on irregular triangular meshes. It is shown that time saving is significant and the ability to handle local refinements is promising for three dimensional simulations around complex geometries or for complete coupling with adaptative mesh refinements technique [11].

After this first validation, effort should be made to improve the artificial viscosity model and the damping properties of the multistage scheme. An alternative which is beeing studied is to use an upwinded scheme instead of the

centered scheme [12], [13].

Acknowledgment

This work was done at Avions Marcel Dassault, Breguet Aviation in the Aerodynamics Studies Department. The author wishes to thank J. Periaux for his help and A. Dervieux from INRIA, Sophia Antipolis, where the author was invited for a month.

REFERENCES

[1] BRANDT, A., ' Multi-level Adaptative Solutions to Boundary Value Problems', Math. Comp. 31, 333-390, 1977.

[2] BILLEY, V., ' Resolution des Equations d'Euler par des Methodes d'Elements Finis', These de docteur de 3e Cycle, Universite de Paris VI, 1984.

[3] STOUFFLET, B., ' Resolution Numerique des Equations d'Euler des Fluides Parfaits Compressibles par des Schemas Implicites en Elements Finis', These de Docteur Ingenieur, Universite de Paris VI, 1984.

[4] DERVIEUX, A., ' Steady Euler Simulation using unstructured meshes ', Von Karman Institute fo Fluid Dynamics, Lecture Series 1985-04, 1985.

[5] [5] ANGRAND, F., DERVIEUX, A., LOTH, L., VIJAYASUNDARAM, G., ' Simulation of Euler Transonic Flows by Means of Explicit Finite Element-type Scheme ', INRIA Research Report, # 250, 1983.

[6] HIRSCH, C., DECONINCK, H., ' A Multigrid Method for the Transonic Full Potential Equation Discretized with Finite Element on an Arbitrary Body Fitted Mesh ', NASA Conference Publication # 2202, 1981.

[7] NI, R. H., ' A Multiple-Grid Scheme for solving the Euler Equations ', AIAA Journal, Vol. 20, # 11, 1982.

[8] JAMESON, A., ' Transonic Flow Calculations ', MAE Report # 1651, Princeton University, 1983.

[9] JAMESON, A., ' Solution of the Euler Equations for two Dimensional Transonic Flow by a Multigrid Method ', MAE Report # 1613, Princeton University, 1983.

[10] JAMESON, A., MAVRIPLIS, D., ' Finite Volume Solution of the Two Dimensional Euler Equations on a Regular Triangular Mesh ', AIAA paper 85-0435, 1985.

[11] PALMERIO, B., BILLEY, V., DERVIEUX, A., PERIAUX, J., ' Self Adaptative Mesh Refinements and Finite Element Methods for Solving the Euler Equations ', Proceedings of the ICFD Conference on "Numerical Methods for Fluid Dynamics",

Reading, 1985.

[12] TURKEL, E., VAN LEER, B., ' Flux Vector Splitting and Runge-Kutta Methods for the Euler Equations', ICASE Report no. 84-27, 1984.

[13] FEZOUI, F., ' Resolution des Equations d'Euler par un Schema de Van Leer en Elements Finis', INRIA Research Report no. 358, 1985.

[14] BERGER, M., J., JAMESON, A., ' An Adaptative Multigrid Method for the Euler Equations', Ninth International Conference on Numerical Methods in Fluid Dynamics, Lecture Notes in Physics, Springer-Verlag, 1985.

[15] USAB, W., MURMAN, E., 'Embedded Mesh Solution of the Euler Equations using a Multiple-Grid Method', AIAA paper # 83-1946-CP, 1983.

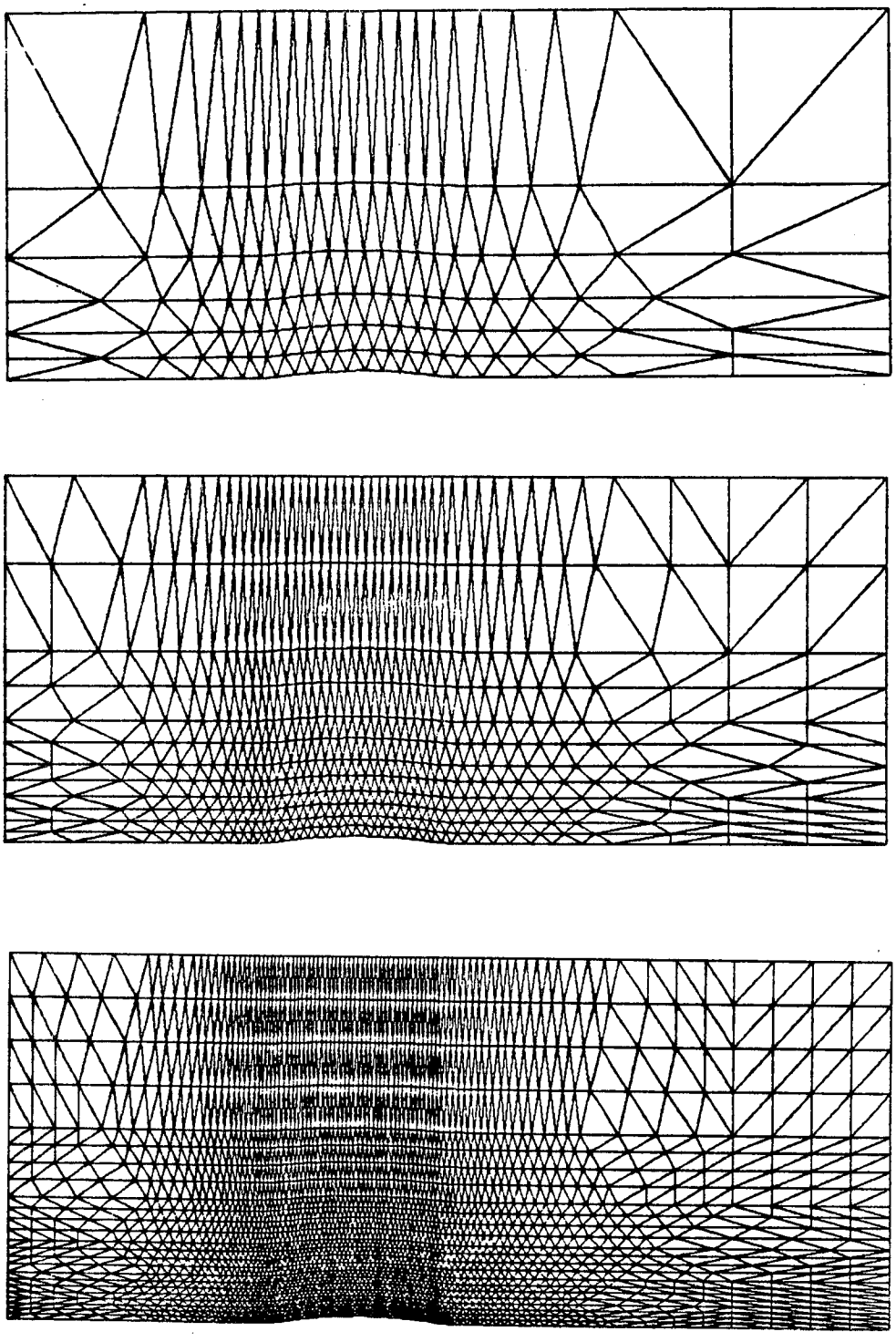

Figure 7 : Successive Grid Levels for Global Multigrid in a Channel with a Bump.

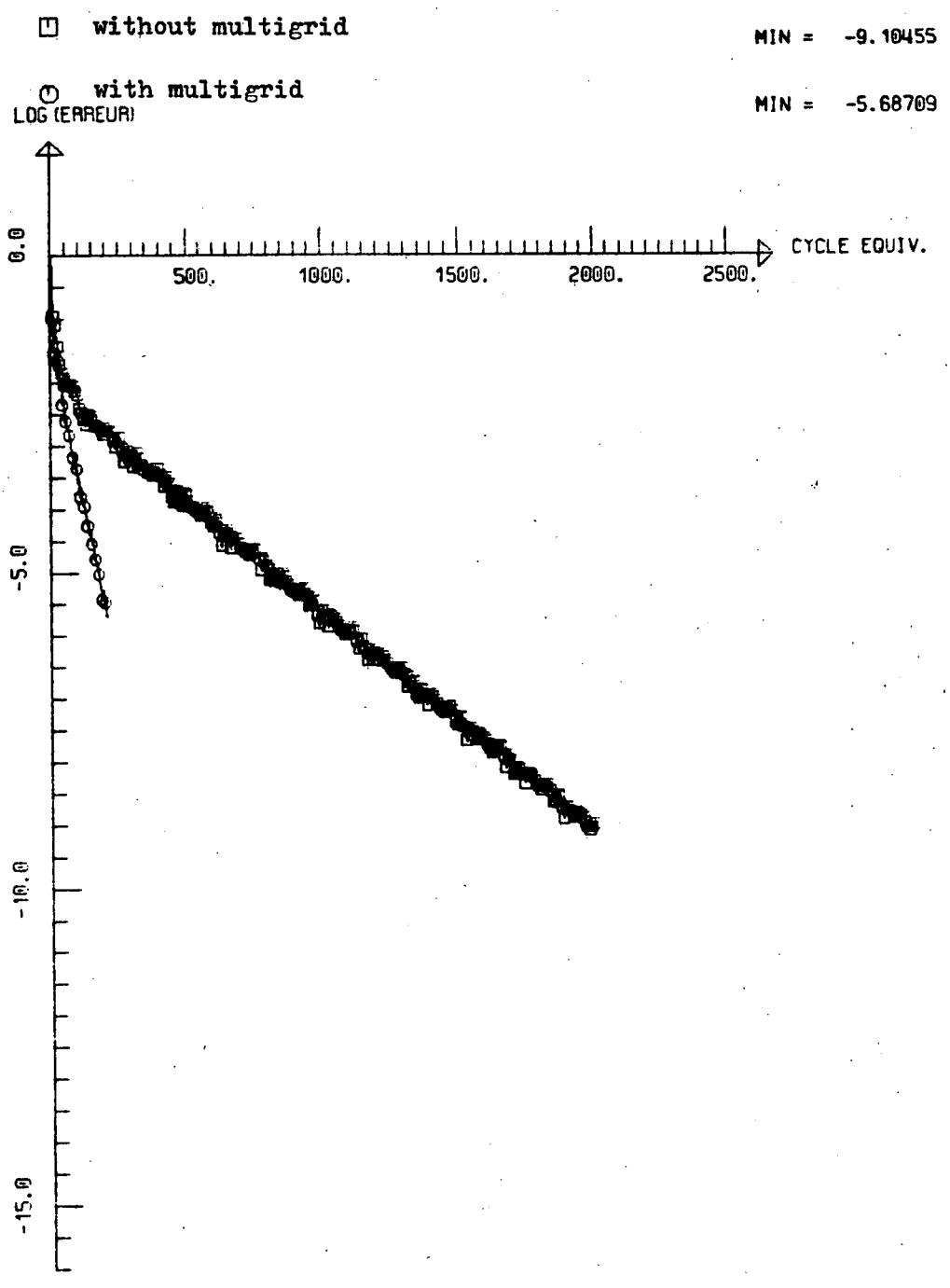

Figure 8 : Convergence History for Subsonic Flow in a Channel with a Bump. M=0.5 .

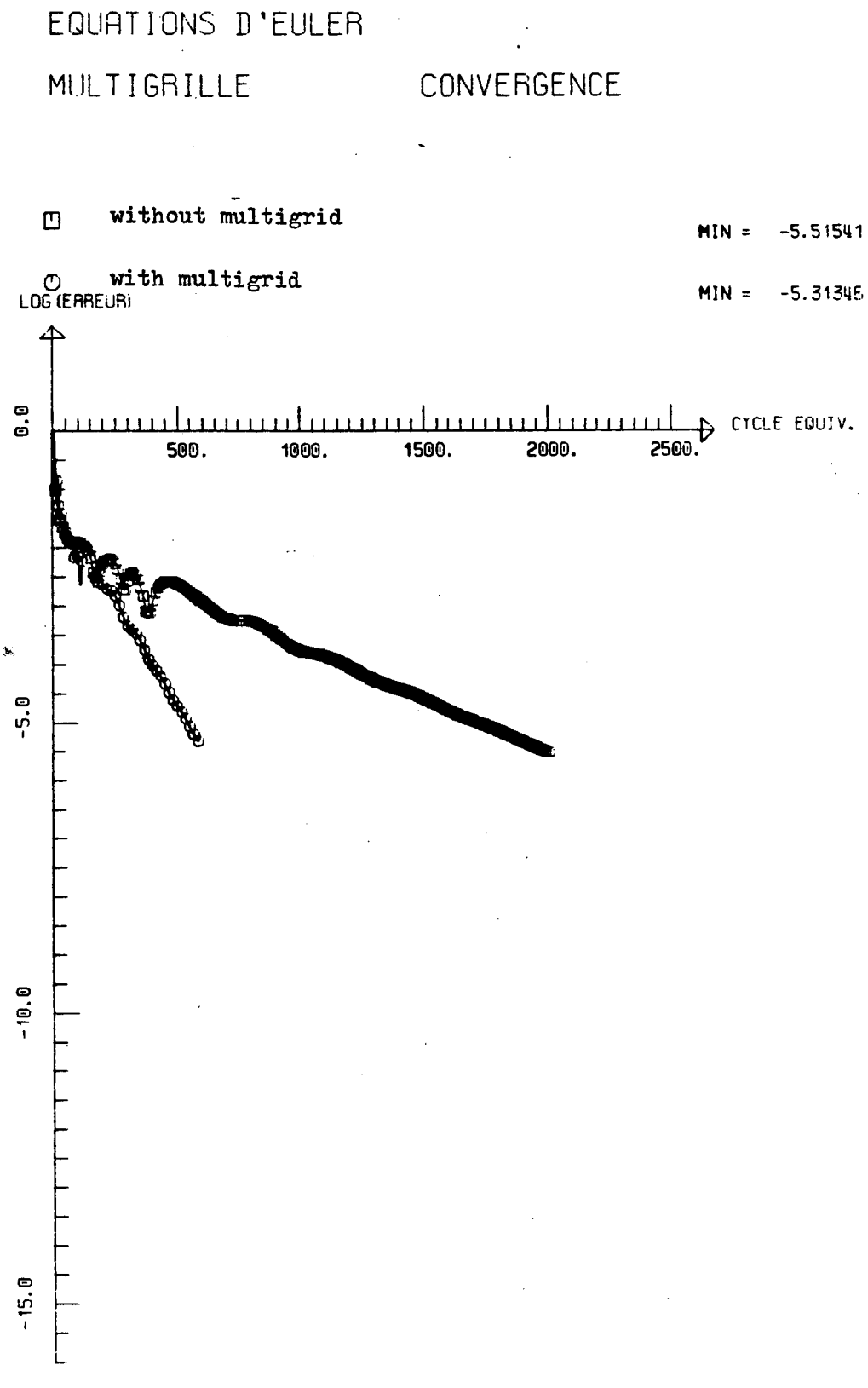

Figure 9 : Convergence History for Transonic Flow in a Channel with a Bump. M = 0.85 .

MAX = 0.56369

MIN = 0.41808

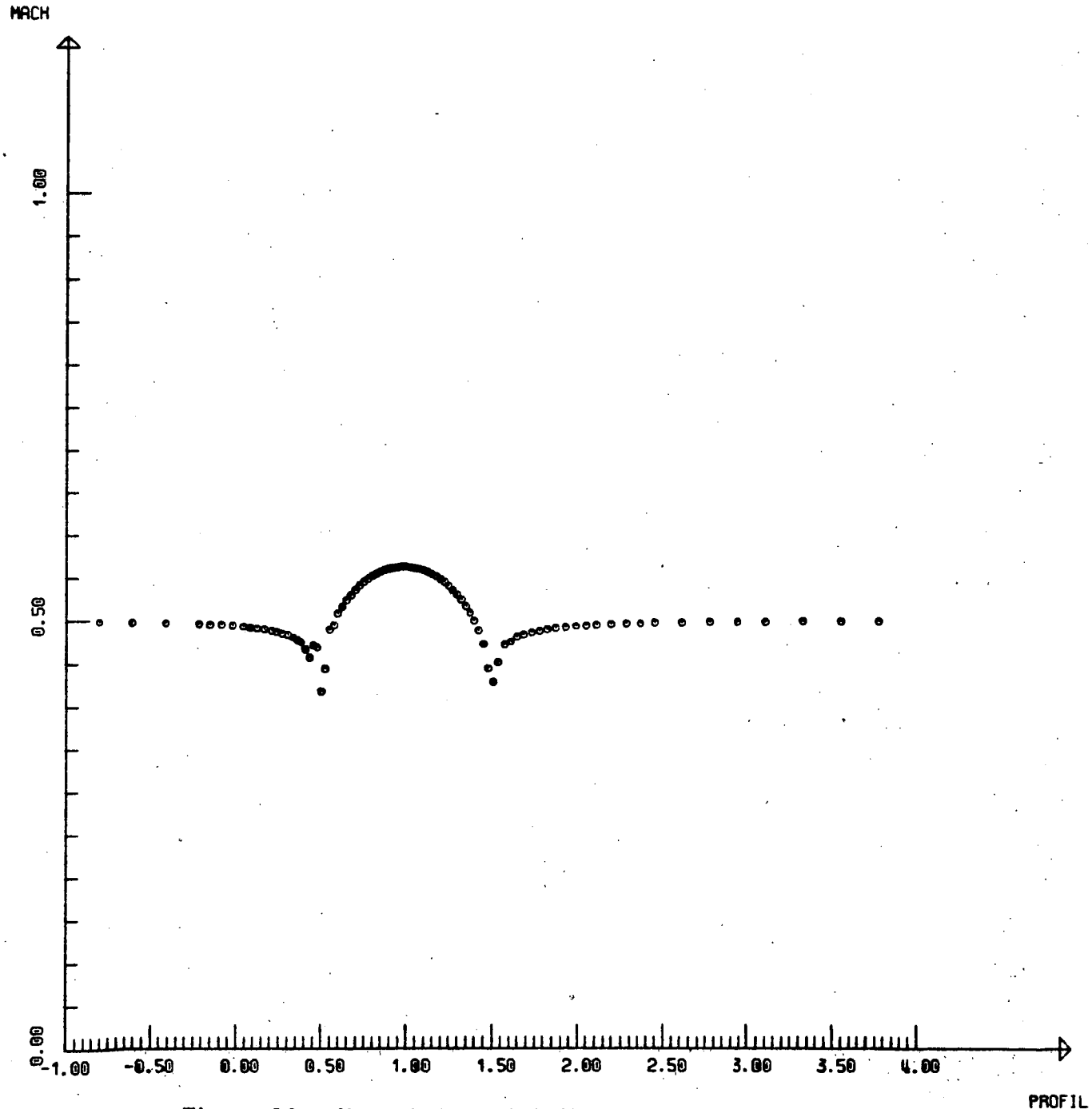

Figure 10 : Mach Number Distribution on the Lower Wall for the Subsonic Case.

MAX = 1.29423

MIN = 0.63761

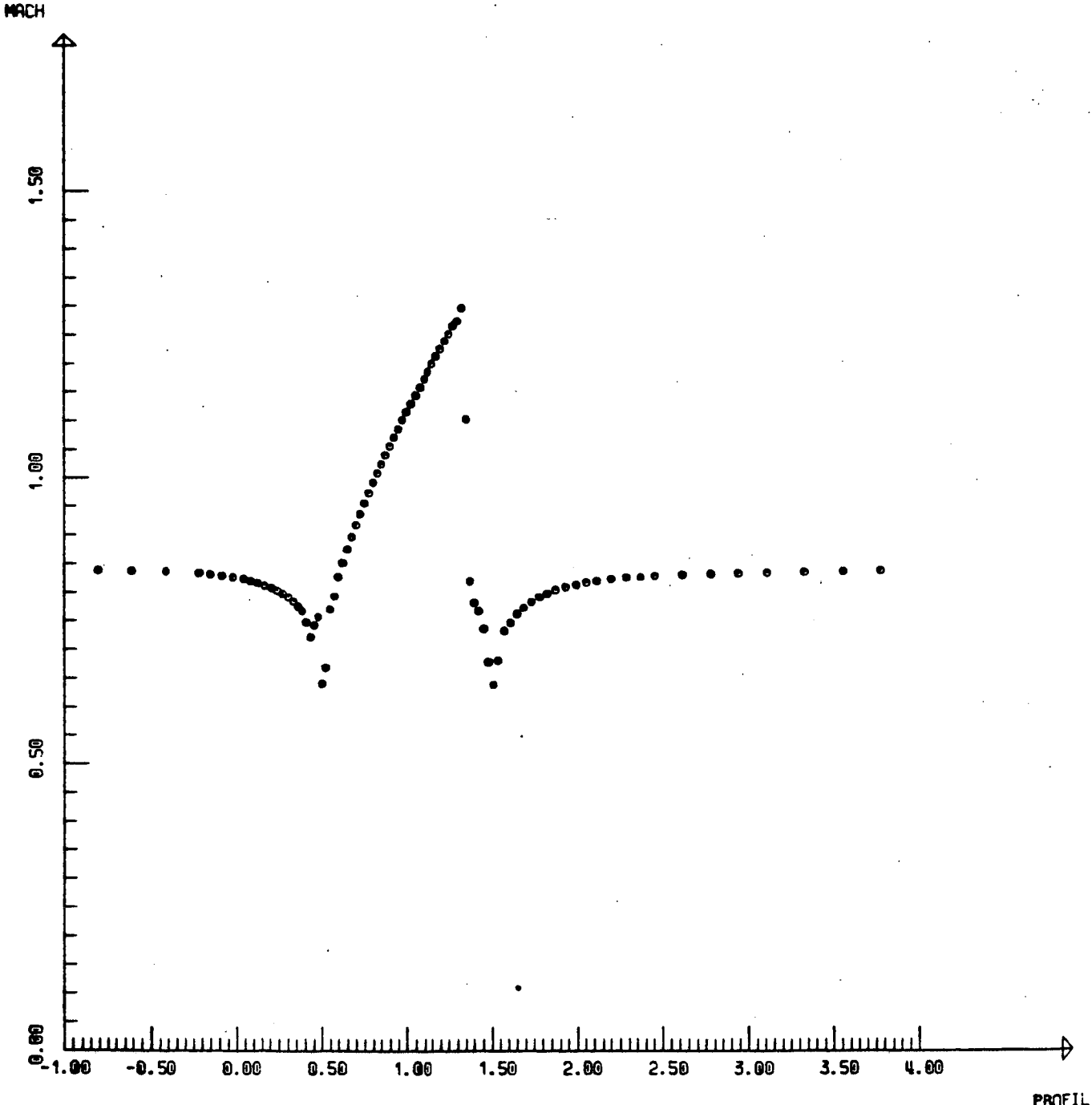

Figure 11 : Mach Number Distribution on the Lower Wall for the Transonic Case.

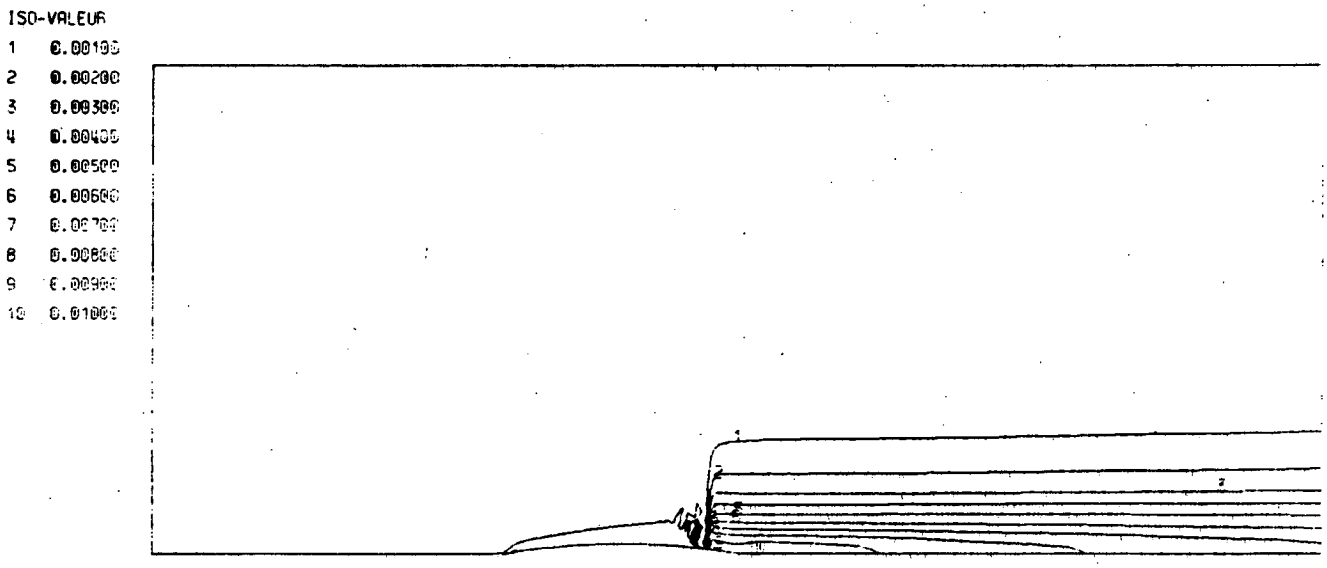

Figure 12 : Entropy Contours for Transonic Case.

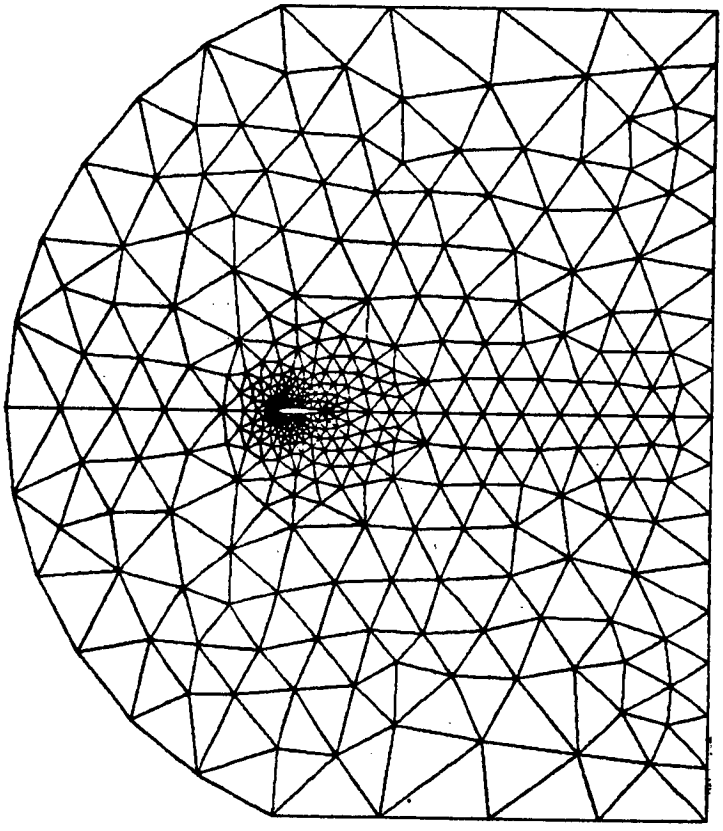

Figure 13 : First Grid Level for a NACA 0012 , Global View, 404 nodes and 738 elements.

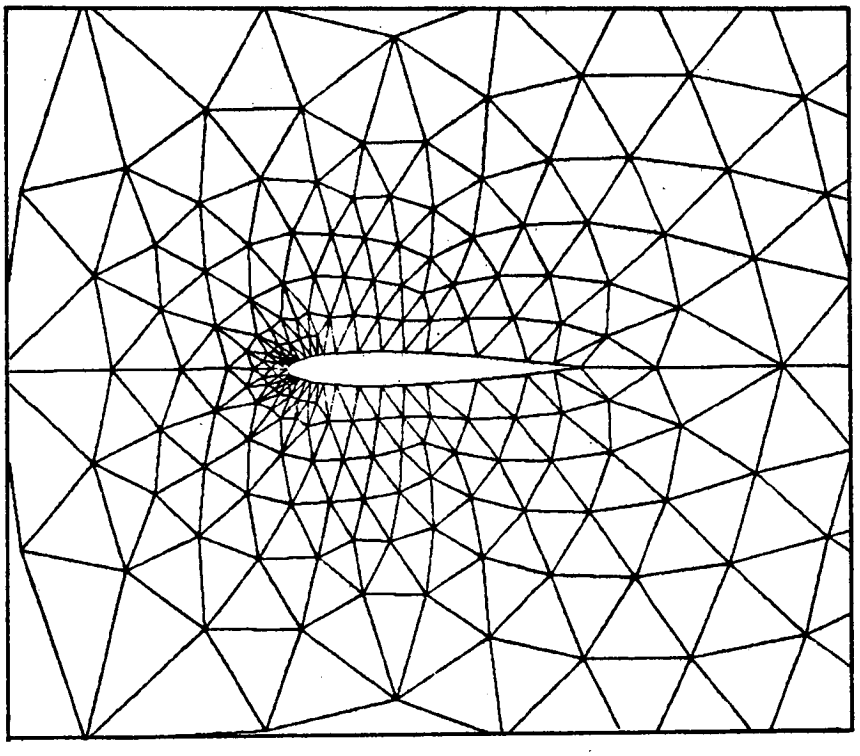

Figure 14 : First Grid Level for a NACA 0012, Local View.

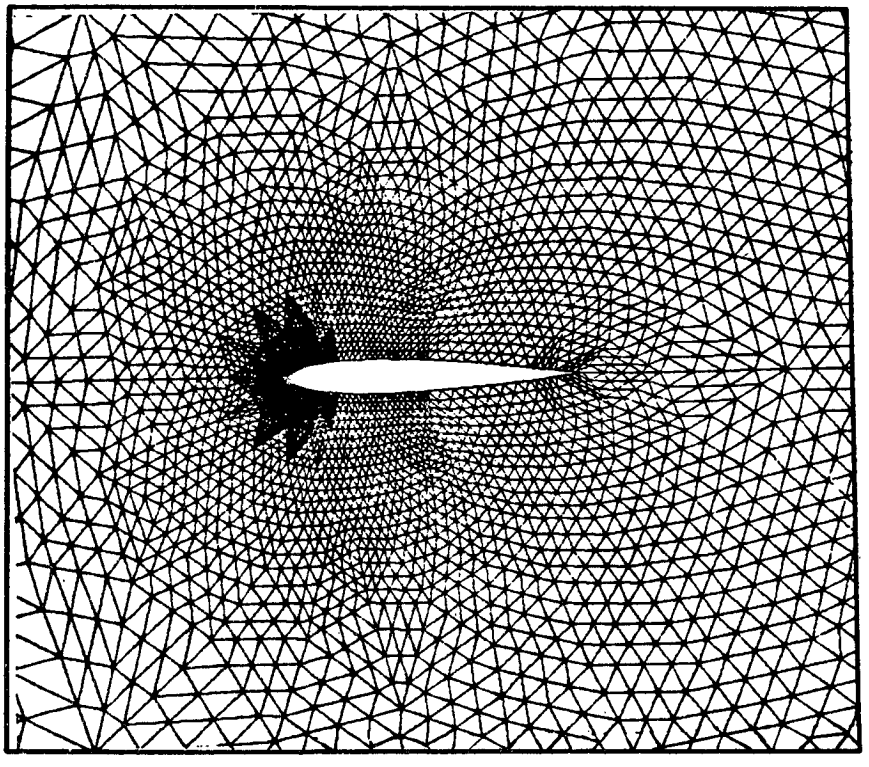

Figure 15 : Third Grid Level for a NACA 0012, Local View, 6044 nodes and 11808 elements.

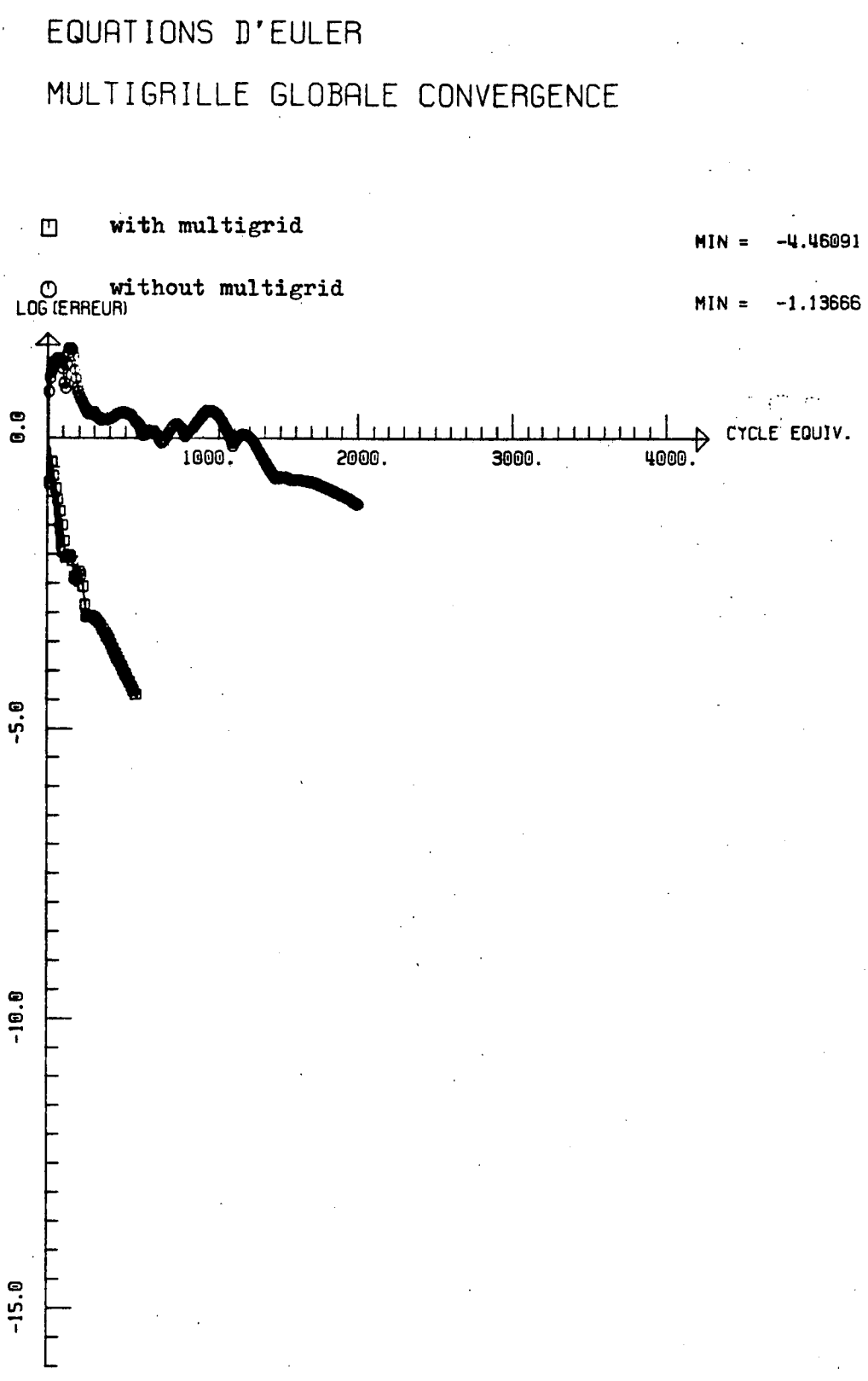

Figure 16 : Convergence History for Lifting Transonic case, M = 0.85 , Alpha = 1°.

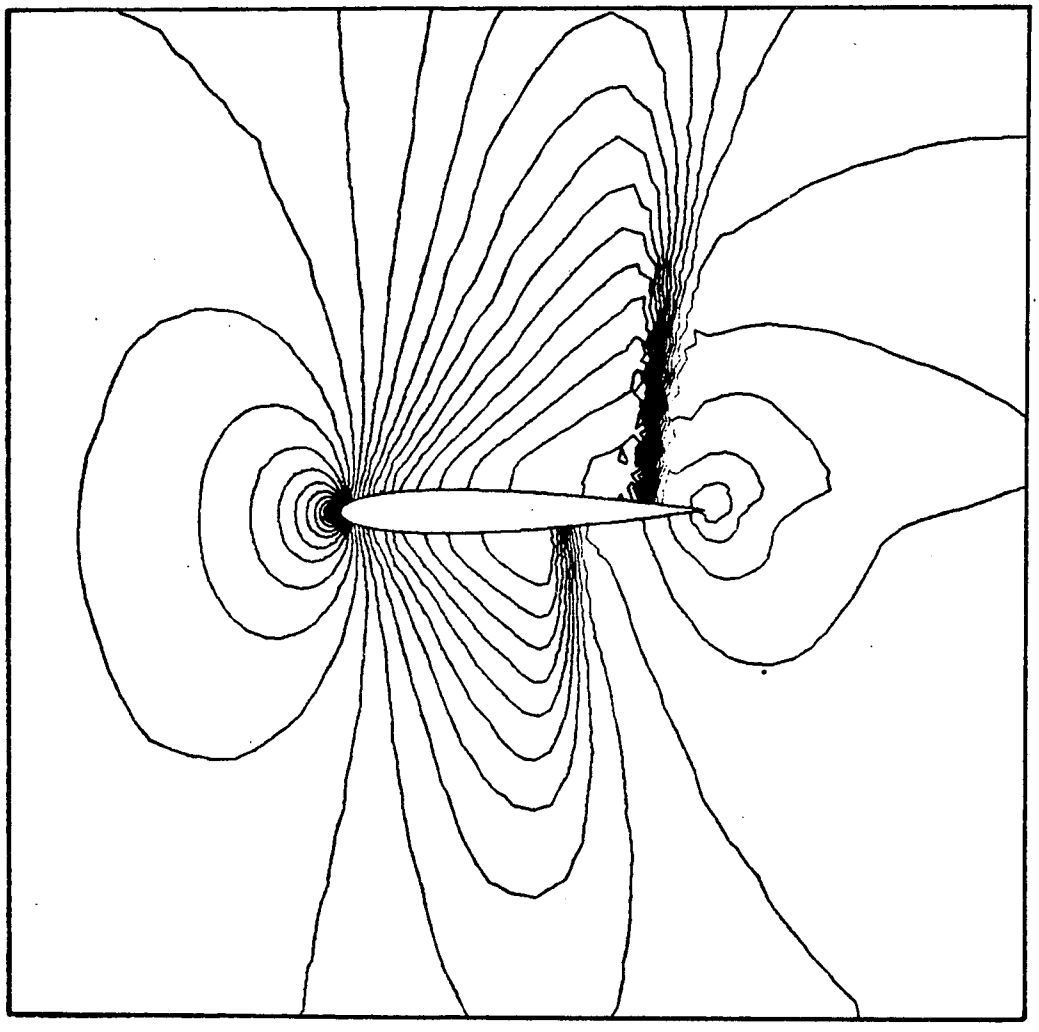

Figure 17 : Mach Contours for Lifting Transonic Case,
$\Delta M = 0.02$.

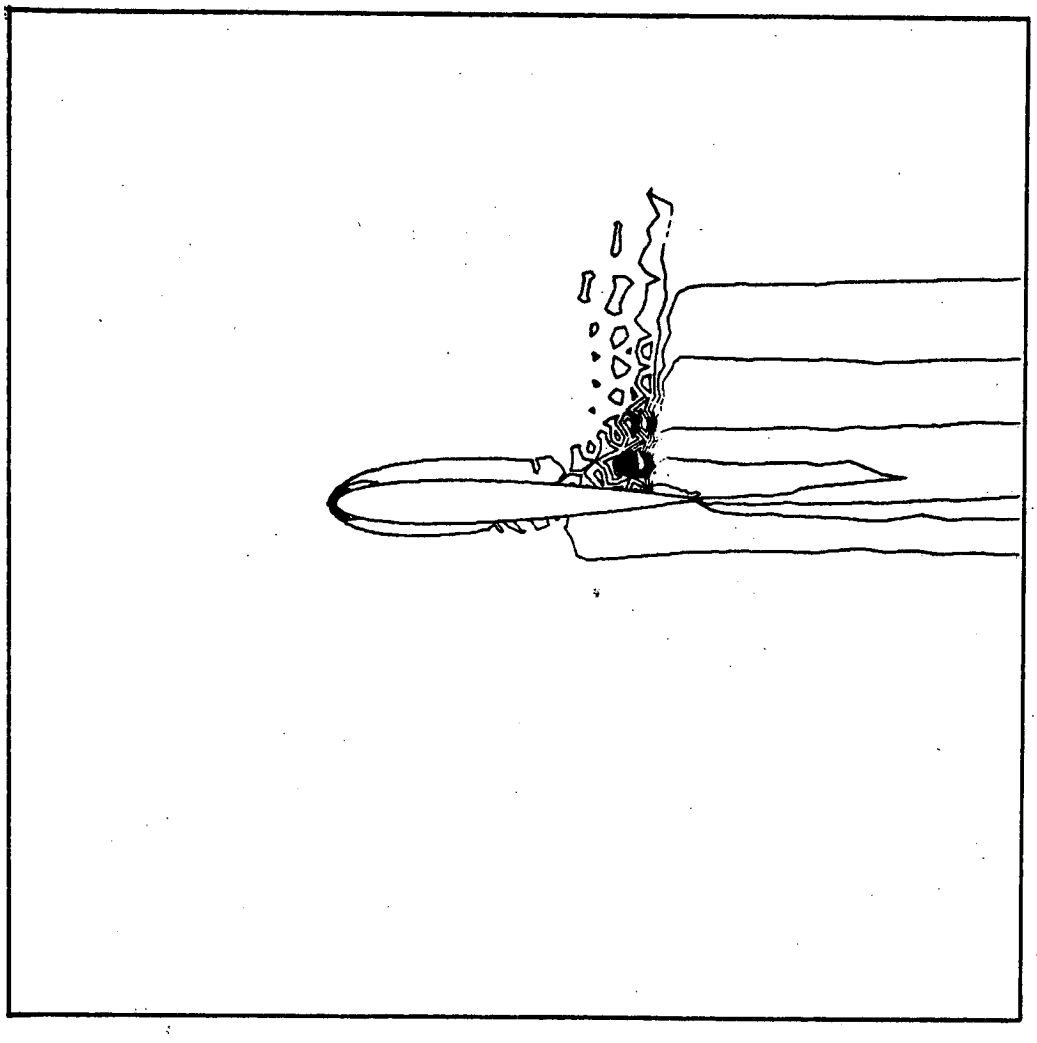

Figure 18 : Entropy Contours for Lifting Transonic Case, $\Delta S = 0.005$.

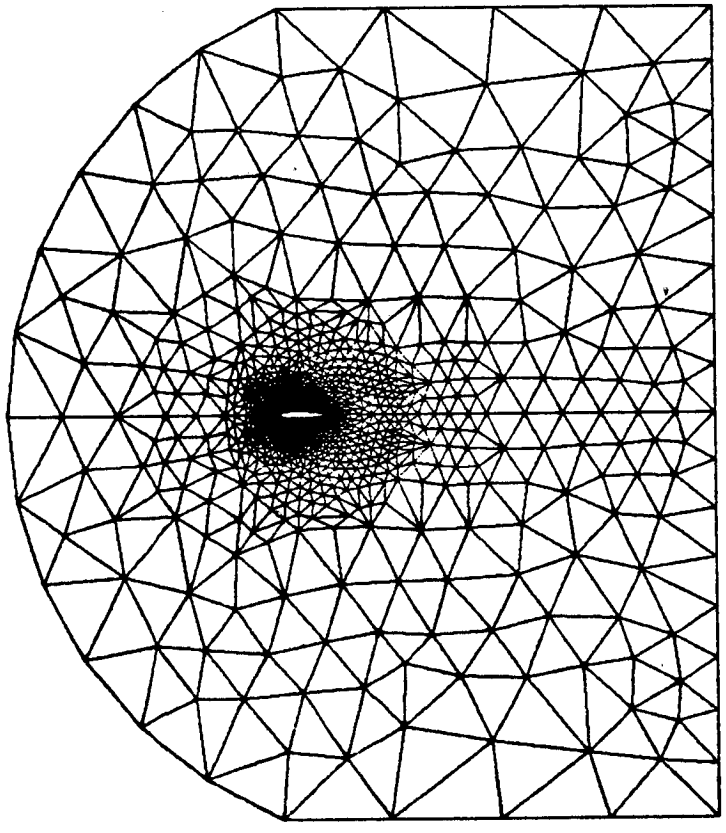

Figure 19 : Second Grid Level for Local Multigrid, Refinement only in a rectangle around the profile. 1125 nodes and 2896 elements.

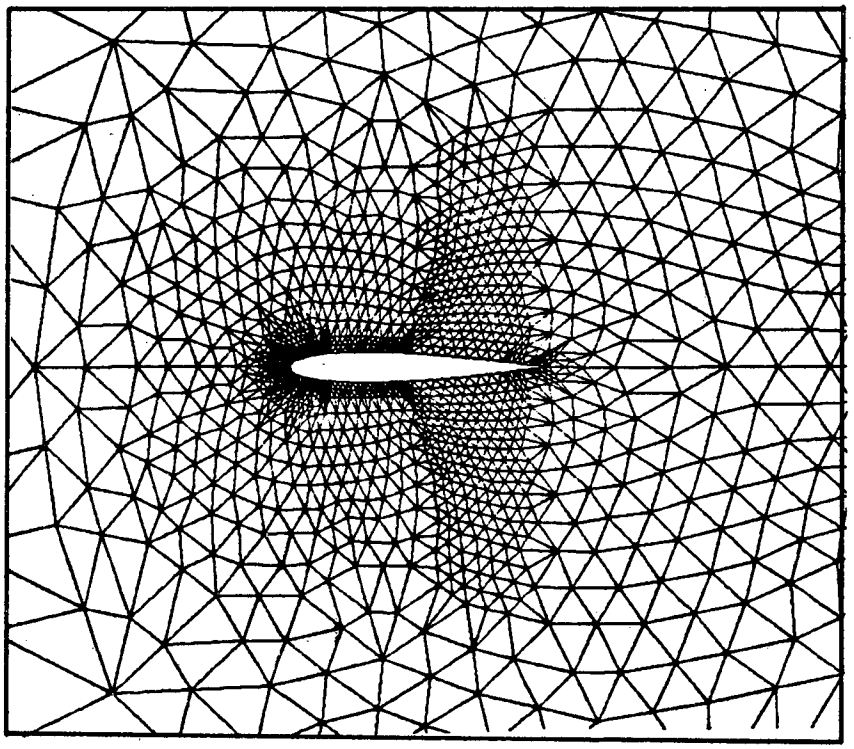

Figure 20 : Third Grid Level for Local Multigrid, Refinement only on the profile and around the Shock, 1669 nodes and 6054 elements.

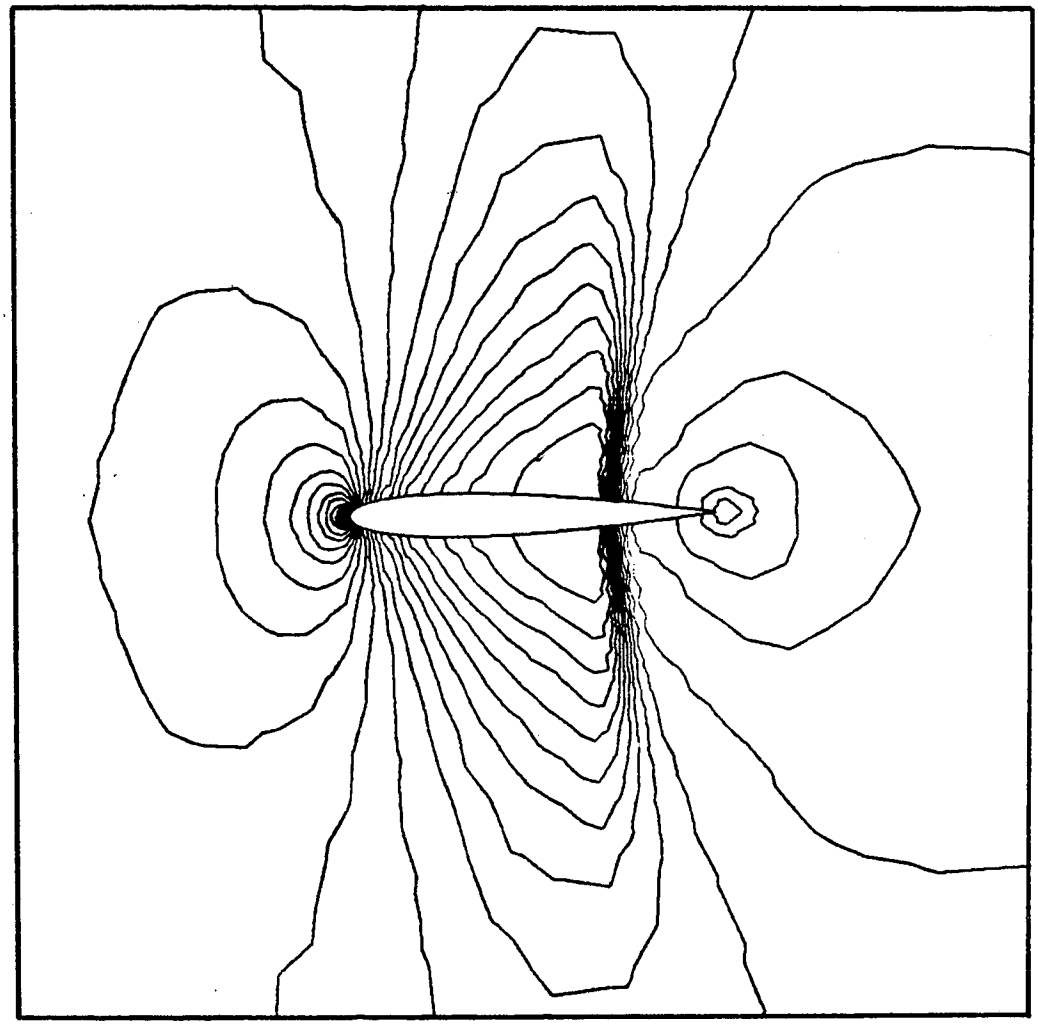

Figure 21 : Mach Number Contours for Local Multigrid
Transonic Case, M = 0.85, Alpha = 0.,
ΔM = 0.02.

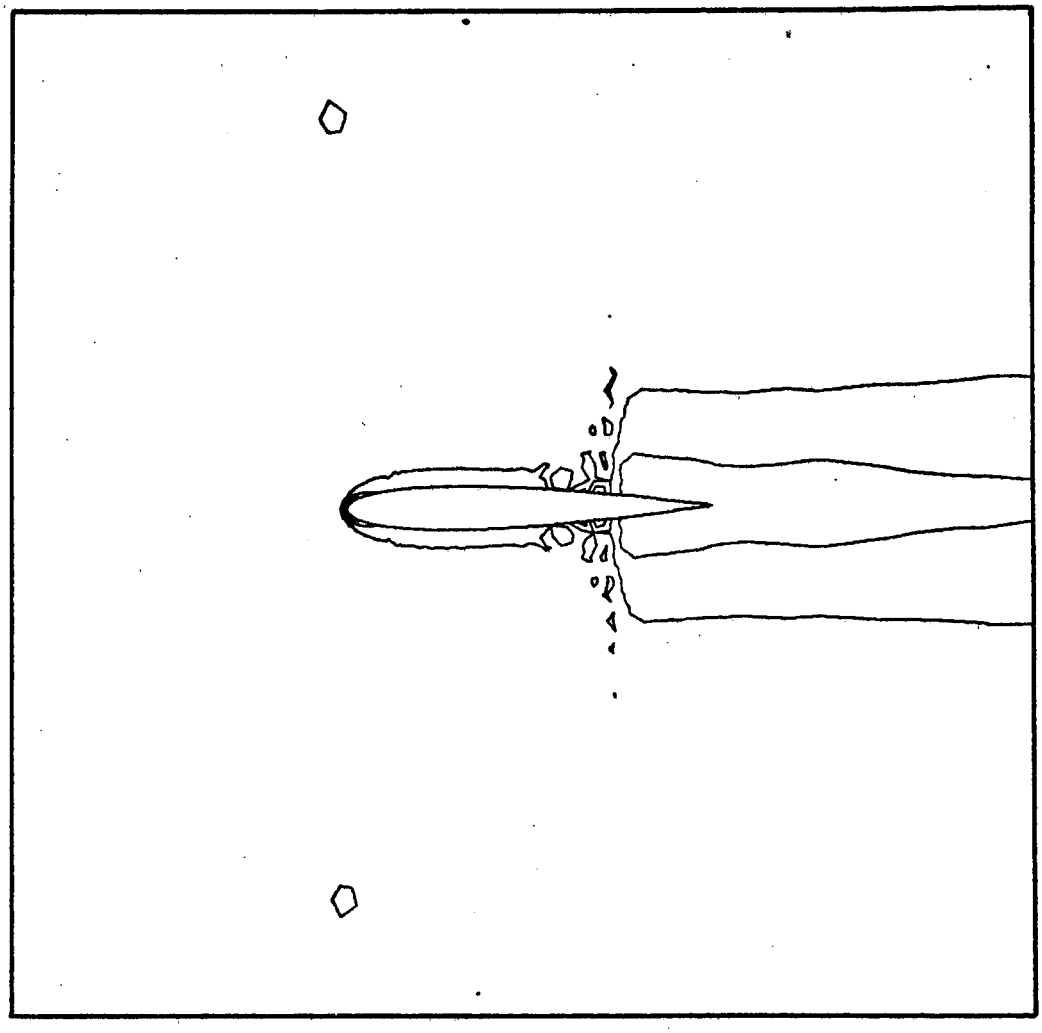

Figure 22 : Entropy Contours for Local Multigrid Transonic Case, $\Delta S = 0.005$.